Ocean Sci. Discuss., 9, 787–833, 2012
www.ocean-sci-discuss.net/9/787/2012/
doi:10.5194/osd-9-787-2012

Ocean Science Discussions

In situ determination of the remote sensing reflectance: an inter-comparison

G. Zibordi[1], K. Ruddick[2], I. Ansko[3], G. Moore[4], S. Kratzer[5], J. Icely[6], and A. Reinart[3]

[1]Institute for Environment and Sustainability, Joint Research Centre, Ispra, Italy
[2]Royal Belgian Institute of Natural Sciences, Management Unit of the North Sea Mathematical Models, Brussels, Belgium
[3]Tartu Observatory, Estonia
[4]Bio-Optika, Crofters, Middle Dimson, Gunnislake, UK
[5]Stockholm University, Department of Systems Ecology, Sweden
[6]Sagremarisco Lda, Vila do Bispo, Portugal

Received: 15 February 2012 – Accepted: 23 February 2012 – Published: 7 March 2012

Correspondence to: G. Zibordi (giuseppe.zibordi@jrc.ec.europa.eu)

Published by Copernicus Publications on behalf of the European Geosciences Union.

Abstract

Inter-comparison of data products from simultaneous measurements performed with independent systems and methods is a viable approach to assess the consistency of products and additionally to investigate uncertainties. Within such a context the inter-comparison called Assessment of In Situ Radiometric Capabilities for Coastal Water Remote Sensing Applications (ARC), was carried out at the Acqua Alta Oceanographic Tower in the Northern Adriatic Sea to explore the accuracy of in situ data products from various in- and above-water optical systems and methods. Measurements were performed under almost ideal conditions including: a stable deployment platform, clear sky, relatively low sun zenith angles and moderately low sea state. Additionally, except for one, all optical sensors involved in the experiment were inter-calibrated through a post-field absolute radiometric calibration performed with the same standards and methods. Inter-compared data products include: spectral water-leaving radiance $L_w(\lambda)$, above-water downward irradiance $E_d(0^+,\lambda)$ and remote sensing reflectance $R_{rs}(\lambda)$. Data products from the various measurement systems/methods were directly compared to those from a single reference system/method. Results for $R_{rs}(\lambda)$ indicate spectrally averaged values of relative differences comprised between −1 and +6 %, while spectrally averaged absolute values of relative differences vary from approximately 6 % for the above-water systems/methods to 9 % for buoy-based systems/methods. The agreement between $R_{rs}(\lambda)$ spectral relative differences and estimates of combined uncertainties of the inter-compared systems/methods is noteworthy.

1 Introduction

Climate studies largely rely on environmental indices derived from remote sensing data (e.g., Behrenfeld et al., 2006; Achard et al., 2002; Kaufman et al., 2002; Stroeve et al., 2007). Satellite ocean color data are also increasingly applied for coastal and inland water management, including water quality monitoring, harmful algal bloom detection

OSD

9, 787–833, 2012

and sediment transport studies (Brando and Dekker, 2003; Stumpf and Tomlinson, 2005, Ruddick et al., 2008). However, the confident use of these data requires the quantification of their uncertainties. This is generally accomplished through the comparison of satellite products with in situ reference measurements. In the case of satellite ocean color, the spectral remote sensing reflectance R_{rs} determined from top-of-atmosphere radiance is the primary data product used for the generation of higher level products such as chlorophyll-*a* concentration (Chl-*a*). As a consequence, access to accurate in situ R_{rs} is essential for the assessment of primary data products from satellite ocean color missions.

In situ R_{rs} data are obtained through in-water and above-water optical measurement systems. Both approaches rely on a number of methods frequently tied to a variety of instruments characterized by different design and performances. This aspect together with a diverse implementation of measurement methods, the application of different processing schemes, and the use of various sources and methods for the absolute radiometric calibration of field instruments, may lead to unpredictable uncertainties significantly affecting the assessment of satellite products.

The quantification and the successive reduction of uncertainties for in situ measurements, is thus a major challenge for ocean color scientists actively involved in field radiometry. Basic tasks include the precise implementation and application of established measurement and analysis methods, and additionally an investigation and quantification of each source of uncertainty in primary data products. Best practice suggests the verification of each measurement and processing step through inter-comparison exercises.

This work summarizes results from a radiometric inter-comparison performed in the Northern Adriatic Sea with the main objective of evaluating the agreement of in situ R_{rs} products determined through the application of independent measurement systems and methods.

OSD
9, 787–833, 2012

2 The inter-comparison

Inter-comparison activities are essential to evaluate the performance of independent measurement methods and also the ability of individuals to properly implement them (e.g., Thome et al., 2008; Hooker et al., 2002a; Barton et al., 2004). A major requirement for inter-comparisons is the need for performing measurements with different systems/methods under almost identical conditions. In the case of optical oceanography, this is better achieved with the use of fixed deployment platforms instead of ships. In fact grounded platforms offer the major advantage of deploying instruments under controlled geometries not affected by superstructure drift and roll. This favourable situation is easily achieved at the Acqua Alta Oceanographic Tower (AAOT) in the Northern Adriatic Sea (e.g., Zibordi et al., 1999; Hooker and Zibordi 2005; Zibordi et al., 2009a).

The inter-comparison activity presented and discussed in this work focuses on a variety of measurement systems and methods currently applied to produce in situ data for the validation of marine primary radiometric products for the Medium Resolution Imaging Spectrometer (MERIS) onboard the Envisat platform of the European Space Agency (ESA). The inter-comparison, called Assessment of In Situ Radiometric Capabilities for Coastal Water Remote Sensing Applications (ARC), was conceived within the framework of the MERIS Validation Team (MVT) and supported by ESA in the context of international activities promoted by the Working Group on Calibration and Validation (WGCV), Infrared and Visible Optical Systems (IVOS) subgroup, of the Committee on Earth Observation Satellites (CEOS).

ARC activities comprise two successive phases carried out during July 2010. In the first phase, field measurements were carried out at the AAOT during four days characterized by favourable illumination and sea state conditions. In the second phase, the optical sensors previously deployed at the AAOT were inter-calibrated at the Joint Research Centre (JRC). This inter-calibration was achieved through the absolute radiometric calibration of the optical sensors by using identical laboratory standards and methodologies, with the exception of one system (see Sect. 3.3.3) also calibrated at

OSD
9, 787–833, 2012

the JRC using the same standards and methodologies, but at a different time. Data products included in the inter-comparison were then all computed from data calibrated (or corrected) using consistently determined radiometric coefficients.

The inter-comparison of data products from different measurement systems and methods is here performed relying on data from a single system/method considered as the reference. Because of the variety of multispectral and hyperspectral sensors included in the inter-comparison, the data analysis has been restricted to the center-wavelengths of major interest for satellite ocean color: 412, 443, 490, 510, 555, and 665 nm. The presentation of results is supported by uncertainty budgets quantified for each system/method.

3 Measurement systems and methods

The ARC inter-comparison includes a variety of in- and above-water measuring systems and methods. To rationalize the description, the basic elements common to generic methods (i.e., in- and above-water) are hereafter summarized, then details on each measurement system and method are provided. It is anticipated that the analysis of results is focused on R_{rs} determined according to its simplest definition (see Sect. 3.1) without applying any correction for the effects of sun zenith on anisotropy of in-water radiance distribution (i.e., the bidirectional effects). In fact the objective of this work is to quantify differences among fundamental radiometric products derived from the application of various systems and methods: the use of the same scheme to account for bidirectional effects would not impact the comparison, while the application of different schemes is out of the scope of the study. In line with such a strategy, the dependence on the viewing geometry of above-water measurements (also depending on the in-water radiance distribution) has been addressed applying an identical correction scheme for all considered methods.

OSD
9, 787–833, 2012

3.1 Overview on in-water measurements

In-water radiometry relies on subsurface continuous or fixed-depth profiles of upwelling radiance $L_u(z,\lambda,t)$, downward irradiance $E_d(z,\lambda,t)$ and usually also upward irradiance $E_u(z,\lambda,t)$ at depths z, wavelength λ and time t. The above-water downward irradiance $E_d(0^+,\lambda,t)$ is also measured to complement the in-water measurements. The in-water measurements are used to extrapolate to 0^- (i.e., just below the water surface) the radiometric quantities which cannot be directly measured because of wave perturbations. Above-water downward irradiance data are used to minimize the effects of illumination changes on in-water radiometric measurements during data collection.

In-water continuous profiles of radiometric quantities result generally from measurements performed with optical sensors operated on profiling systems (e.g., winched or free-fall). Due to wave focusing and defocusing, the accuracy of sub-surface radiometric products depends on the sampling depth-interval and on the depth-resolution (Zaneveld et al., 2001; D'Alimonte et al., 2010). Thus highly accurate in-water radiometric products can only be determined by sampling near the surface (especially in coastal regions, due to possible vertical non-homogeneities in the optical properties of seawater) and, by producing a large number of measurements per unit depth not significantly affected by tilt (Zibordi et al., 2004a).

In-water fixed-depth profiles mostly result from the use of optical sensors operated on buoys at nominal depths. These buoy-based systems generally provide the capability of measuring $L_u(z,\lambda,t)$, $E_d(z,\lambda,t)$ and possibly $E_u(z,\lambda,t)$ at multiple depths (typically between 1 and 10 m), in addition to $E_d(0^+,\lambda,t)$. By neglecting the effects of system tilt, the accuracy of radiometric products determined with buoy-based systems is a function of the discrete depths selected for the optical sensors, the acquisition rate and the duration of logging intervals (Zibordi et al., 2009a).

The same data reduction process is in principle applicable to both fixed-depth and continuous profile radiometric data $\Im(z,\lambda,t)$ (i.e., $L_u(z,\lambda,t)$, $E_u(z,\lambda,t)$ and $E_d(z,\lambda,t)$). The initial step, leading to minimization of perturbations created by illumination change

OSD
9, 787–833, 2012

during data collection, is performed according to

$$\Im_0(z,\lambda,t_0) = \frac{\Im(z,\lambda,t)}{E_d(0^+,\lambda,t)} E_d(0^+,\lambda,t_0) \quad (1)$$

where $\Im_0(z,\lambda,t_0)$ indicates radiometric quantities as if they were all taken at the same time t_0, and $E_d(0^+,\lambda,t_0)$ specifies the above-water downward irradiance at time t_0 (with t_0 generally chosen to coincide with the beginning of the acquisition sequence).

Omitting the variable t, the sub-surface quantities $\Im_0(0^-,\lambda)$ (i.e., $L_u(0^-,\lambda)$, $E_u(0^-,\lambda)$ and $E_d(0^-,\lambda)$) are then determined as the exponentials of the intercepts resulting from the least-squares linear regressions of $\ln\Im_0(z,\lambda)$ versus z within the extrapolation interval identified by $z_1 < z < z_2$ and chosen to satisfy the requirement of linear decay of $\ln\Im_0(z,\lambda)$ with depth. The negative values of the slopes of the regression fits are the so-called diffuse attenuation coefficients $K_\Im(\lambda)$ (i.e. $K_l(\lambda)$, $K_u(\lambda)$ and $K_d(\lambda)$) for the selected extrapolation interval.

The radiometric quantity of major relevance here is the so-called water-leaving radiance $L_w(\lambda)$, in units of $\mathrm{mW\,cm^{-2}\,\mu m^{-1}\,sr^{-1}}$. This is the radiance leaving the sea quantified just above the surface from

$$L_w(\lambda) = 0.543\, L_u(0^-,\lambda)\,. \quad (2)$$

where the factor 0.543, derived assuming the seawater refractive index is independent of wavelength (Austin, 1974), accounts for the reduction in radiance from below to above the water surface.

A second radiometric quantity central to this study is the remote sensing reflectance $R_{rs}(\lambda)$ in units of $\mathrm{sr^{-1}}$ given by

$$R_{rs}(\lambda) = \frac{L_w(\lambda)}{E_d(0^+,\lambda)}\,. \quad (3)$$

$R_{rs}(\lambda)$ is thus a quantity corrected for illumination conditions depending on sun zenith angle, sun-earth distance and atmospheric diffuse transmittance (Mueller et al., 2002).

OSD
9, 787–833, 2012

3.2 Overview on above-water measurements

Above-water methods generally rely on measurements of: (i) total radiance from above the sea $L_T(\theta,\Delta\phi,\lambda)$ (that includes water-leaving radiance as well as sky- and sun-glint contributions); (ii) the sky radiance $L_i(\theta',\Delta\phi,\lambda)$; and usually also $E_d(0^+,\lambda)$. The measurement geometry is defined by the sea-viewing zenith angle θ, the sky-viewing zenith angle θ' and the difference between sun and sensor azimuth angles, $\Delta\phi = \phi_0 - \phi$ (Deschamps et al., 2004; Hooker et al., 2004; Zibordi et al., 2004b). The accurate determination of $L_w(\lambda)$ then depends on the capability of minimizing glint contributions through the use of suitable measurement geometries (Mobley, 1999), and additionally, the application of statistical filtering schemes to L_T (Hooker et al., 2002a; Zibordi et al., 2002), or physically-based correction methods relying on known reflectance properties of seawater in the near-infrared spectral region (Ruddick et al., 2006), or alternatively polarisers to directly reduce sky- and sun-glint (Fougnie et al., 1999).

In the case of non-polarized systems, measurements of $L_T(\theta,\Delta\phi,\lambda)$ and $L_i(\theta',\Delta\phi,\lambda)$ for the determination of $L_w(\lambda)$ are generally performed at $\theta = 40$ and $\theta' = 140^\circ$, with $\Delta\phi$ chosen between $+90$ and $+135^\circ$ or alternatively -90 and -135°. The value of $\Delta\phi = \pm 135^\circ$ is considered the most appropriate (see Mobley, 1999). However, its application is more likely to lead to measurements significantly affected by the shadow casted by deployment superstructures.

The water-leaving radiance $L_w(\theta,\Delta\phi,\lambda)$ for a given viewing geometry is computed as

$$L_w(\theta,\Delta\phi,\lambda) = L_T(\theta,\Delta\phi,\lambda) - \rho(\theta,\Delta\phi,\theta_0,W)L_i(\theta',\Delta\phi,\lambda)\,, \quad (4)$$

where $\rho(\theta,\Delta\phi,\theta_0,W)$ is the sea surface reflectance that can be theoretically determined as a function of the measurement geometry identified by $\theta,\Delta\phi,\theta_0$, and of the sea state conveniently expressed through the wind speed, W (measured at 10 m a.s.l.).

The water-leaving radiance $L_w(\lambda)$ for a nadir-view direction is then determined by

$$L_w(\lambda) = L_w(\theta,\phi,\lambda)\frac{\Re_0}{\Re(\theta,W)}\frac{Q(\theta,\Delta\phi,\theta_0,\lambda,\tau_a,\mathrm{IOP})}{Q_n(\theta_0,\lambda,\tau_a,\mathrm{IOP})}\,, \quad (5)$$

OSD
9, 787–833, 2012

where $\Re(\theta,W)$ and $\Re_0$ (i.e., $\Re(\theta,W)$ at $\theta = 0$) account for the sea surface reflectance and refraction, and depend mainly on θ and W. The spectral quantities $Q(\theta,\Delta\phi,\theta_0,\lambda,\tau_a,\text{IOP})$ and $Q_n(\theta_0,\lambda,\tau_a,\text{IOP})$ are the Q-factors at viewing angle θ and at nadir (i.e., $\theta = 0$), respectively, describing the anisotropic distribution of the in-water radiance. The Q-factor (Morel et al., 2002) varies with $\theta,\Delta\phi$, sun zenith θ_0 and, the atmospheric optical properties (conveniently expressed as a function of the aerosol optical thickness τ_a) and finally the seawater inherent optical properties IOPs (conveniently expressed as a function of Chl-*a* in oceanic waters).

The remote sensing reflectance is then computed from Eq. 3 using measured or theoretical values of $E_d(0^+,\lambda)$.

3.3 Details on individual measurement systems and methods

Systems and methods included in the ARC inter-comparison are listed in Table 1 together with the main input parameters required for data processing, and the institutes responsible for data collection, processing and quantifying system/method uncertainties.

3.3.1 WiSPER

The Wire-Stabilized Profiling Environmental Radiometer (WiSPER) is a winched system deployed through a custom-built profiling rig at a speed of 0.1 m s^{-1} at 7.5 m from the main structure of the AAOT. The L_u, E_u and E_d optical sensors are mounted at approximately the same depth (see Zibordi et al., 2004a). The rigidity and stability of the rig is maintained through two taut wires anchored between the tower and the sea bottom. The immovability of the AAOT and the relatively low deployment speed ensure an accurate optical characterization of the subsurface water layer.

WiSPER sensors include three OCI-200 for $E_u(z,\lambda,t)$, $E_d(z,\lambda,t)$ and $E_d(0^+,\lambda,t)$ and one OCR-200 for $L_u(z,\lambda,t)$ measurements. These sensors, manufactured by Satlantic Inc. (Halifax, Canada), provide data at 6 Hz in seven spectral bands 10 nm

OSD
9, 787–833, 2012

wide centered at 412, 443, 490, 510, 555, 665 and 683 nm. The L_u sensor has approximately 18° in-water full-angle field of view (FAFOV). Each WiSPER measurement sequence includes data from down- and up-casts.

WiSPER data are processed in agreement with the scheme presented in Sect. 3.1. Radiometric products for ARC inter-comparison have been determined choosing an extrapolation interval of 0.3–3.0 m. Additional processing includes the application of corrections for superstructure perturbations (Doyle and Zibordi, 2002), self-shading of L_u and E_u sensors (Gordon and Ding, 1992; Zibordi and Ferrari, 1995; Mueller et al., 2002) and non-cosine response of the above-water E_d sensor (Zibordi and Bulgarelli, 2007). In addition to the diameter of the sensors, the application of these corrections requires spectral values of the above-water diffuse to direct irradiance ratio (r) and, subsurface seawater absorption (a) and beam-attenuation (c) coefficients (all regularly measured during each WiSPER deployment).

An analysis of uncertainties of WiSPER $R_{rs}(\lambda)$ from ARC measurements, performed assuming each contribution independent from the others, indicates values in the range of approximately 4–5 % in the selected spectral region (see Table 2). The uncertainty sources considered here are: (i) uncertainty of the absolute in-air radiance calibration (Hooker et al., 2002b) and immersion factor (Zibordi, 2006) for the L_u sensor (i.e., 2.7 % and 0.5 %, respectively, composed statistically); (ii) uncertainty of the correction factors applied for removing self-shading and tower-shading perturbations computed as 25 % of the applied corrections; (iii) uncertainty of the in-air irradiance calibration of the above-water E_d sensor (Hooker et al., 2002b) and uncertainties of the correction applied for the non-cosine response of the related irradiance collectors (Zibordi and Bulgarelli, 2007) (i.e., 2.3 % and 1 %, respectively, composed statistically); (iv) uncertainty in the extrapolation of sub-surface values due to wave perturbations and, changes in illumination and seawater optical properties during profiling cumulatively quantified as the average of the variation coefficient of $R_{rs}(\lambda)$ from replicate measurements.

OSD
9, 787–833, 2012

It is noted that the proposed uncertainty analysis accounts for fully independent calibrations of E_d and L_u sensors (i.e., as obtained with different lamps and laboratory set-ups). The use of the same calibration lamp and set-up would lead to a reduction of approximately 1 % of the quadrature sum of spectral uncertainties for WiSPER $R_{rs}(\lambda)$.

The quality of WiSPER radiometric products is traced through quality indices determined during data processing. These include: temporal changes in illumination conditions as caused by cloudiness and quantified through the standard deviation of $E_d(0^+,\lambda,t)$ at each λ; potential difficulties in the determination of subsurface extrapolated quantities flagged by a relatively small number of measurements per unit depth; significant differences between $E_u(z,\lambda,t_0)/L_u(z,\lambda,t_0)$ at different depths in the extrapolation interval, and large differences between $E_d(0^-,\lambda,t_0)$ and $E_d(0^+,\lambda,t_0)$; poor illumination conditions, as resulting with high sun zenith angles or cloudiness, both quantified through values of the diffuse to direct ratio $r(\lambda)$ exceeding a threshold. These quality-indices, recorded as an integral part of the radiometric data set, are used to comprehensively qualify data products. The low deployment speed of WiSPER and the almost ideal sky and sea-state conditions characterizing the ARC measurements made all the collected data applicable for the inter-comparison.

3.3.2 TACCS

The Tethered Attenuation Chain Colour Sensors (TACCS) manufactured by Satlantic Inc. consists of an above-water E_d sensor mounted on a buoy, an upwelling L_u sensor at a depth z_0 of approximately 0.5 m depth and a chain of four in-water E_d sensors at increasing depths z. A weight suspended at the bottom of the chain stabilises the system against wave action. TACCS offers the advantage of easy system deployment from small boats and the possibility of being operated at distances minimizing ship perturbations. Additionally, $L_u(z_0,\lambda,t)$ data taken relatively close to the surface can be averaged over time to minimize the effects of wave focussing and defocusing. The main disadvantage is the reduced depth resolution with respect to profilers, thus

OSD
9, 787–833, 2012

requiring a careful quality check of data to exclude cases affected by near-surface optical non-homogeneities.

Individual measurement sequences comprise collection of $L_u(z_0,\lambda,t)$, $E_d(z_i,\lambda,t)$ and $E_d(0^+,\lambda,t)$ during intervals of three minutes. Measurement sequences are retained and corrected using equation 1 for the effects of illumination change during data collection, when the range of $E_d(0^+,\lambda,t)$ is not greater than 2.5 % (sea-state 0–1), 3.0 % (sea-state 1–2) or 4 % (sea-state 4): essentially, the variability should be consistent with wave action, rather than changes in illumination which have a longer frequency. Derived $L_u(z_0,\lambda,t_0)$ and $E_d(z,\lambda,t_0)$ are then averaged over the three minutes interval to determine time-averaged $\bar{E}_d(z,\lambda,t_0)$ and $\bar{L}_u(z_0,\lambda,t_0)$ values, respectively.

Log transformed $\bar{E}_d(z,\lambda,t_0)$ are then applied to compute $K_d(\lambda)$ through least-squares linear regressions. By assuming $K_l(\lambda) = K_d(\lambda)$, subsurface $L_u(0^-,\lambda)$ is then obtained from

$$L_u(0^-,\lambda) = \frac{\bar{L}_u(z_0,\lambda,t_0)}{e^{-z_0 K_d(\lambda)}} \quad (6)$$

Quality checks for $L_u(0^-,\lambda)$ include the evaluation of R^2 determined from the regression of $\bar{E}_d(z,\lambda,t_0)$ at depths z and the visual inspection of $\bar{E}_d(z,490,t_0)$ profile data. If R^2 and the vertical profile of log-transformed $\bar{E}_d(z,490,t_0)$ indicate non-homogeneity of the optical properties in the water column, then the lowest depth(s) are removed from the processing. These steps aim at ensuring the validity of the hypothesis of homogeneous seawater optical properties between the surface and at least the second measurement depth.

Self-shading corrections of $L_u(0^-,\lambda)$ data are performed following the methodology detailed by Mueller et al. (2002). Input quantities are: the total seawater absorption coefficient $a(\lambda)$ assumed equal to $K_d(\lambda)$; the diameter of the L_u sensor (by neglecting the marginal effects of the surface float; Moore et al., 2010); and the diffuse to direct irradiance ratio $r(\lambda)$ calculated from simulated data using the model of Bird and Riordan (1986) with extra-atmospheric irradiance from Thullier et al. (2003) and aerosol optical

OSD
9, 787–833, 2012

thickness $\tau_a(\lambda)$ from collocated sun-photometric measurements.

Two TACCS systems were deployed during the ARC inter-comparison: one owned and managed by Stockholm University in collaboration with Bio-Optika (identified as TACCS-S); and the second by Sagrimisco Lda also in collaboration with Bio-Optika (identified as TACCS-P). Although the two TACCS systems have different radiometric configurations, the mechanical design is almost identical.

TACCS-S

TACCS-S measures $E_d(0^+,\lambda,t)$ at 443, 490 and 670 nm, and $E_d(z,\lambda,t)$ at 490 nm at the nominal depths of 2, 4, 6 and 8 m. Measurements of $L_u(z_0,\lambda,t)$ are performed at 412, 443, 490, 510, 560, 620 and 670 nm at the nominal depth $z_0 = 0.5$ m with an in water FAFOV of approximately 20°. All sensors have a 10 nm bandwidth. The acquisition rate is 0.5 Hz.

TACCS-S does not have tilt sensors but, when carefully balanced in water, combined $x-y$ tilt of the above-water E_d sensor remains below 5° at sea state 0–1.

Since $E_d(0^+,\lambda,t)$ is only measured at 443, 490 and 670 nm, simulated irradiances (computed using the same model utilized for the determination of r) are normalized to the actual $E_d(0^+,\lambda,t)$ to determine values at 412, 510, 560 and 620 nm.

Similarly, since $K_d(\lambda)$ is only measured at 490 nm, spectral values of $K_d(\lambda)$ at the relevant center-wavelengths are determined from measurements of $a(\lambda)$ and $c(\lambda)$ following Kirk (1994) using

$$K_d(\lambda) = \mu_0^{-1}\left[a(\lambda)^2 + (g_1\mu_0 - g_2)a(\lambda)b(\lambda)\right]^{0.5} \quad (7)$$

where $b(\lambda) = c(\lambda) - a(\lambda)$, μ_0 is the mean cosine of the refracted solar beam just below the sea surface, and, g_1 and g_2 constants depending on the phase function. For the processing of ARC data, constant values are $\mu_0 = 0.86$, and $g_1 = 0.425$, $g_2 = 0.19$ corresponding to the Petzold (1972) phase function. It is assumed that these parameters provide the correct spectral shape of $K_d(\lambda)$, although its absolute value may be biased due to dependence of μ_0 on θ_0.

OSD
9, 787–833, 2012

The analysis of uncertainties for TACCS-S $R_{rs}(\lambda)$ from ARC measurements indicates values in the range of approximately 7–8 % (see Table 3). Considered uncertainty sources are: (i) uncertainty of the absolute in-air radiance calibration (Hooker et al., 2002b) and immersion factor (Zibordi, 2006) of the L_u sensor (i.e., 2.7 % and 0.5 %, respectively, composed statistically); (ii) uncertainty of the correction factors applied for removing self-shading perturbations in $L_u(0^-,\lambda)$ computed as 35 % of the applied corrections; (iii) uncertainty of the in air absolute irradiance calibration of the above-water E_d sensor (Hooker et al., 2002) and non-cosine response of the related irradiance collectors (Zibordi and Bulgarelli, 2007) (i.e., 2.3 % and 2 %, respectively, composed statistically); (iv) uncertainty in the determination of $E_d(0^+,\lambda)$ at missing center-wavelengths estimated by calculating $E_d(0^+,\lambda)$ using the model of Bird and Riordan (1986) with $\tau_a(500) = 0.45$ (average for measurements performed during the field activities) and by bracketing the Ångström exponent α to 0.0 and 2.0; (v) uncertainties due to the assumption of $K_l(\lambda) = K_d(\lambda)$ resulting from the quadrature sum of 1.7 %, average difference between $K_d(\lambda)$ and $K_l(\lambda)$ determined through Hydrolight (Mobley, 1998) simulations using the specific TACCS E_d and L_u sensor depths, and of approximately 1.7 % per 100 nm due to spectral extrapolation as estimated from actual measurements; (vi) uncertainties due to geometrical effects estimated from simulations assuming: tilt of 5 ° for the above-water E_d sensor, relative sun-sensor of 180 °, $\theta_0 = 45°$, $r(\lambda)$ computed with $\tau_a(500) = 0.45$, and $\alpha = 1.39$ as resulting from measurements performed during field activities; (vii) uncertainty in the extrapolation of sub-surface values due to wave perturbations and, changes in illumination and seawater optical properties during profiling cumulatively quantified as the average of the variation coefficient of $R_{rs}(\lambda)$ from replicate measurements.

Uncertainties do not take into account potential shading by the cable of the in-water E_d sensors. This is supported by the assumption that this perturbation similarly affects measurements at all depths and thus does not significantly influence the determination of $K_d(\lambda)$. No uncertainty has been assigned to the nominal depths of in-water E_d sensors assumed known to within ±2 cm under calm sea.

OSD
9, 787–833, 2012

Finally, in view of the inter-comparison analysis, it is anticipated that differences between TACCS-S center-wavelengths at 560 and 670 nm with respect to the reference ones at 555 and 665 nm, are neglected.

TACCS-P

TACCS-P has hyper-spectral sensors for $E_d(0^+,\lambda,t)$ and $L_u(z_0,\lambda,t)$ measurements performed in the spectral range of 350–800 nm with resolution of 11 nm. The L_u sensor has in-water FAFOV of approximately 18°. $E_d(z_i,\lambda,t)$ is measured at 412, 490, 560 and 665 nm, with a bandwidth of 10 nm at nominal depths of 2, 4, 8 and 16 m. Sampling rate is typically 2–3 Hz, although it may vary depending on illumination conditions.

Since $K_d(\lambda)$ is only determined at 412, 490, 560 and 665 nm, at the other relevant center-wavelengths it is determined with the following scheme. The value of Chl-*a* is estimated from $K_d(490)$ by inverting Eq. (9) from Morel and Antoine (1994) duly taking into account the diffuse attenuation coefficient of pure seawater. Then the same equation with the estimated Chl-*a* is applied to determine the diffuse attenuation coefficient of seawater (pure seawater excluded). The derived $K_d(\lambda)$ spectrum is subsequently normalised to the experimental values determined at 412, 490, 560 and 665 nm.

$E_d(0^+,\lambda,t)$ is calculated by two methods depending on tilt values during the sampling period. The value of $E_d(0^+,\lambda,t)$ is kept unchanged if the combined $x-y$ tilt value is less than 2°. Otherwise a correction is applied by assuming that the diffuse irradiance is unaffected by tilt (i.e., by ignoring the sky radiance distribution) according to

$$E_d(0^-,\lambda,t) = \frac{E_d(0^-,\lambda,t,\theta_s)}{1+\frac{f(\theta_0,\theta_s)-1}{1+r(\lambda)}} \quad (8)$$

where $E_d(0^-,\lambda,t,\theta_s)$ indicates the data to be corrected through the factor $f(\theta_0,\theta_s)$ given by

$$f(\theta_0,\theta_s) = \frac{\cos(\theta_s)}{\cos(\theta_0)} \quad (9)$$

OSD
9, 787–833, 2012

with θ_s the apparent angle of the sun at the collector of the irradiance sensor.

This correction, however, only applies to θ_s less than 8° (chosen on the basis of trials performed under stable illumination conditions). In fact when the tilt becomes high the radiance from the sea surface may add large perturbations, especially in the anti-solar direction.

The analysis of uncertainties for TACCS-P $R_{rs}(\lambda)$ from ARC measurements indicates values in the range of approximately 6–7 % (see Table 4). Considered uncertainty sources are: (i) uncertainty of the absolute in-air radiance calibration (Hooker et al., 2002b) and immersion factor (Zibordi, 2006) of the L_u sensor (i.e., 2.7 % and 0.5 %, respectively, composed statistically); (ii) uncertainty in the correction factors applied for removing self-shading perturbations in $L_u(z_0,\lambda,t)$ computed as 35 % of the applied corrections; (iii) uncertainty of the in air absolute irradiance calibration of the above-water E_d sensor (Hooker et al., 2002b) and the non-cosine response of the related irradiance collectors (Zibordi and Bulgarelli, 2007) (i.e., 2.3 % and 2 %, respectively, composed statistically); (iv) uncertainties due to the assumption of $K_l(\lambda) = K_d(\lambda)$ resulting from the quadrature sum of 1.7 %, average difference between $K_d(\lambda)$ and $K_l(\lambda)$ determined through Hydrolight (Mobley, 1998) simulations using the specific TACCS E_d and L_u sensor depths, and of approximately 1.7 % per 100 nm due to spectral extrapolation as estimated from actual measurements; (v) uncertainties due to geometrical effects estimated from simulations assuming: tilt of 5° for the above-water E_d sensor, $\theta_0 = 45°$, relative sun-sensor of 180°, $r(\lambda)$ computed using $\tau_a(500) = 0.45$ and $\alpha = 1.39$ from measurements performed during the field activities; (vi) uncertainty due to the extrapolation of sub-surface values due to wave perturbations and, changes in illumination and seawater optical properties during profiling (cumulatively quantified as the average of the variation coefficient of $R_{rs}(\lambda)$ from replicate measurements).

3.3.3 SeaPRISM

The SeaWiFS Photometer Revision for Incident Surface Measurements (SeaPRISM) is a modified CE-318 sun-photometer (CIMEL, Paris) that has the capability of performing

OSD
9, 787–833, 2012

autonomous sequences of measurements for the determination of $L_w(\lambda)$ at a number of center-wavelengths including 412, 443, 488, 531, 551, 670 nm (Zibordi et al., 2009c). SeaPRISM measurements performed with a FAFOV of 1.2° every 30 min include: (i) a series of direct sun irradiance measurements $E_s(\theta_0, \phi_0, \lambda)$ acquired to determine the atmospheric optical thickness $\tau_a(\lambda)$ used for the theoretical computation of $E_d(0^+, \lambda)$; and (ii) a sequence of 11 sea-radiance measurements for determining $L_T(\theta, \Delta\phi, \lambda)$ and of 3 sky-radiance measurements for determining $L_i(\theta', \Delta\phi, \lambda)$. These sequences are serially repeated for each λ with $\Delta\phi = 90$, $\theta = 40$ and $\theta' = 140°$. The larger number of sea measurements, when compared to sky measurements, is required because the higher environmental noise (mostly produced by wave perturbations) affecting the former measurements during clear sky.

Values of $R_{rs}(\lambda)$ are determined from SeaPRISM measurements in agreement with basic principles provided in Sect. 3.2. An additional element is the need to minimize the effects of wave perturbations in $L_T(\theta, \Delta\phi, \lambda)$ and possibly the effects of cloud perturbations in $L_i(\theta', \Delta\phi, \lambda)$. This is achieved by deriving these values from the average of independent measurements satisfying strict filtering criteria (Zibordi et al., 2009c).

Finally, as already anticipated, the value of $E_d(0^+, \lambda)$ is quantified theoretically under the assumption of clear sky. Specifically,

$$E_d(0^+, \lambda) = \frac{D^2 t_d(\lambda) \cos\theta_0}{E_0(\lambda)}, \quad (10)$$

where D^2 accounts for the variations in the sun-earth distance as a function of the day of the year, $t_d(\lambda)$ is the atmospheric diffuse transmittance computed from measured values of $\tau_a(\lambda)$ (Gordon and Clark, 1981), and $E_0(\lambda)$ is the average extra-atmospheric sun irradiance (Thuillier et al., 2003).

Quality flags are applied at the different processing levels to remove poor determinations of $L_{wn}(\lambda)$. These include checking for (see, Zibordi et al., 2009c): cloud contamination; high variance of multiple sea- and sky-radiance measurements; elevated differences between pre- and post-calibrations of the SeaPRISM system; and

OSD
9, 787–833, 2012

spectral inconsistency of the normalized-water leaving radiance $L_{wn}(\lambda)$ (where $L_{wn}(\lambda) = R_{rs}(\lambda)E_0(\lambda)$).

It is recalled that SeaPRISM data, handled through the Ocean Color component of the Aerosol Robotic Network (AERONET-OC, Zibordi et al., 2009c), are mostly intended to support satellite ocean color validation activities. Because of this, to minimize the effects of differences in center-wavelengths between satellite and SeaPRISM data products, a band-shift correction scheme has been developed for the latter. These corrections are performed relying on a bio-optical model requiring Chl-*a* and IOP values estimated through regional empirical algorithms applied to spectral ratios of $L_{wn}(\lambda)$ (see Zibordi et al., 2009b). Band-shift corrections have then been applied to SeaPRISM data products contributing to the ARC inter-comparison to match the reference center-wavelengths.

SeaPRISM is the only system deployed during the ARC experiment that was not immediately post-field inter-calibrated. This is explained by its continuous use at the AAOT for periods of 6–12 months. However, pre- and post deployment calibrations performed at the JRC with the same standards and methods applied during ARC, indicated differences typically within 0.6 % during a 9 months period.

Estimated uncertainties of SeaPRISM $R_{rs}(\lambda)$ data for the ARC experiment are approximately 4–5 % in the blue-green spectral regions and 10 % in the red (see Table 5). These have been determined accounting for contributions from: (i) uncertainty of the absolute radiance calibration (Hooker et al., 2002b) for L_T and L_i sensors, but neglecting sensitivity changes during deployment which should contribute less than 0.2 % when assuming a linear change with time between pre- and post-deployment calibrations; (ii) uncertainty of corrections for the off-nadir viewing geometry computed as 25 % of the applied correction factors; (iii) variability in specific parameters required for the determination of $R_{rs}(\lambda)$ (taken from Zibordi et al., 2009c and estimated from multi-annual measurements accounting for changes in wind speed, sea surface reflectance, atmospheric diffuse transmittance); (iv) uncertainty in $E_0(\lambda)$ estimated by assuming rectangular 10 nm bandwidths and ±1 nm uncertainty in center-wavelengths;

OSD
9, 787–833, 2012

and finally, (v) environmental perturbations (e.g., wave effects, changes in illumination and seawater optical properties during measurements) quantified as the average of the variation coefficient obtained from $R_{rs}(\lambda)$ values from replicate measurements.

The uncertainty related to band-shift corrections has not been accounted for the uncertainty budget. However, an evaluation of band-shift corrections applied to SeaPRISM data to match center-wavelengths of various satellite sensors indicated average values of a few percent (Zibordi et al., 2006). Thus, the uncertainty affecting these values is expected to be a small fraction of the applied corrections and consequently to not significantly impact the uncertainty budget proposed for SeaPRISM $R_{rs}(\lambda)$.

3.3.4 TRIOS

Above-water TriOS systems (TriOS Mess- und Datentechnik GmbH, Germany) are composed of two RAMSES ARC-VIS hyperspectral radiometers measuring $L_T(\theta, \Delta\phi, \lambda)$ and $L_i(\theta', \Delta\phi, \lambda)$ radiance and one RAMSES ACC-VIS for $E_d(0^+, \lambda)$ irradiance. Measurements are performed in the 400–900 nm spectral range with resolution of about 10 nm for the output data. The nominal FAFOV of radiance sensors is 7°.

The basic measurement method applied during ARC is that developed by Ruddick et al. (2006, see the main paper and web appendices) based on the generic *Method 1* described in the Ocean Optics Protocols (Mueller et al., 2002).

L_T and L_i sensors are simultaneously operated on the same frame with identical azimuth plane and, $\theta = 40$ and $\theta' = 140°$, respectively. Measurement sequences are performed with user-definable intervals and frequencies, and integration time varying automatically between 8 ms and 4 s depending on the brightness of the target. During ARC, the deployment frame was adjusted for each measurement sequence to satisfy the requirement of $\Delta\phi = 135°$ (or occasionally of $\Delta\phi = 90°$ chosen to avoid superstructure perturbations).

OSD
9, 787–833, 2012

Details on data processing, including measurement selection, averaging and quality checks are described in Ruddick et al. (2006) (web appendix 1: http://aslo.org/lo/toc/vol_51/issue_2/1167a1.pdf). A few elements on data processing are however provided here for completeness.

Following Ruddick et al. (2006) and in agreement with Sect. 3.2 and Sect. 3.1, the remote sensing reflectance $R'_{rs}(\theta,\Delta\phi,\lambda)$ for individual $L_T(\theta,\Delta\phi,\lambda)$ and $L_i(\theta',\Delta\phi,\lambda)$ measurements is computed as

$$R'_{rs}(\theta,\Delta\phi,\lambda) = \frac{L_T(\theta,\Delta\phi,\lambda) - \rho(W)L_i(\theta',\Delta\phi,\lambda)}{E_d(0^+,\lambda)} \quad (11)$$

where $\rho(W)$ indicates the sea surface reflectance during clear sky conditions, solely expressed as a function of W (in units of $m\,s^{-1}$)

$$\rho(W) = 0.0256 + 0.00039W + 0.000034W^2 . \quad (12)$$

Minimization of perturbations due to wave effects is then achieved through the so-called *turbid water near-infrared (NIR) similarity correction* (Ruddick et al., 2005) by determining the departure from the NIR similarity spectrum with

$$\varepsilon = \frac{\alpha \cdot R'_{rs}(\theta,\Delta\phi,\lambda_1) - R'_{rs}(\theta,\Delta\phi,\lambda_2)}{\alpha - 1} \quad (13)$$

where wavelengths λ_1 and λ_2 are chosen in the near infrared and α set accordingly from Table 2 of Ruddick et al. (2006).

The NIR-similarity corrected remote sensing reflectance $R_{rs}(\theta,\Delta\phi,\lambda)$ is then calculated from

$$R_{rs}(\theta,\Delta\phi,\lambda) = R'_{rs}(\theta,\Delta\phi,\lambda) - \varepsilon \quad (14)$$

where the correction is assumed spectrally invariant. The corresponding NIR-similarity corrected water-leaving radiance is calculated as

$$L_w(\theta,\Delta\phi,\lambda) = E_d(0^+,\lambda)R_{rs}(\theta,\Delta\phi,\lambda) \quad (15)$$

OSD
9, 787–833, 2012

A number of data products (i.e., 5) are then averaged to obtain the NIR-similarity corrected $\bar{L}_w(\theta,\Delta\phi,\lambda)$.

For ARC measurements a viewing angle correction is also applied to $\bar{L}_w(\theta,\Delta\phi,\lambda)$ in agreement with Eq. (5) to determine $L_w(\lambda)$. The values of Chl-*a* required for such a correction were estimated using a regional band-ratio algorithm (Berthon and Zibordi, 2004).

Two TriOS systems were deployed during the ARC experiment: one owned and handled by the Management Unit of the North Sea Mathematical Models (identified as TRIOS-B) and the other by Tartu Observatory (identified as TRIOS-E). The two systems are equivalent but measurements have been performed independently and reduced by applying slightly different schemes, corresponding to the standard practice of the two institutions and with some differences in the approach for uncertainty estimate. These elements are separately presented in the following sub-sections.

Data for inter-comparisons have been constructed by linearly interpolating quality checked products at the reference center-wavelengths.

TRIOS-B

$E_d(0^+,\lambda)$, $L_T(\theta,\Delta\phi,\lambda)$ and $L_i(\theta',\Delta\phi,\lambda)$ are simultaneously acquired for 10 min taking measurements every 10 s. Calibrated data are quality checked for incomplete and for individual measurements differing by more than 25 % from the neighbouring ones. In the case of ARC data, quality checking led to the rejection of 1 % of measurements. The NIR-similarity correction is then performed using $\lambda_1 = 780$ nm, $\lambda_2 = 870$, and $\alpha = 1.91$ (Ruddick et al., 2006).

Estimated uncertainties of $R_{rs}(\lambda)$ for TRIOS-B approximately vary between 4 and 6 % in the spectral range of interest (see Table 6). The considered uncertainty sources are: (i) uncertainty of system calibration determined assuming the same irradiance standard is utilized for the absolute calibration of the E_d, L_T, and L_i sensors, and thus only accounting for effects of mechanical setup, inadequate baffling and reference plaque uncertainties (see Hooker et al., 2002b); (ii) uncertainty due to straylight effects

OSD
9, 787–833, 2012

quantified through the application of laboratory characterizations performed for RAMSES E_d, L_T and L_i sensors (Ansko, unpublished); (iii) polarization effects quantified as the maximum sensitivity to polarization determined through laboratory characterizations for RAMSES L_T and L_i sensors (Ruddick, unpublished); (iv); effects of non-cosine response of the above-water E_d collector determined from laboratory measurements (Ruddick, unpublished); (v) uncertainty in sky-light correction quantified in agreement with Ruddick et al. (2006) as a function of the uncertainty in $\rho(W)$; (vi) uncertainty in the correction for off-nadir viewing angle quantified as 25 % of the applied corrections, and exhibiting different values than those proposed for SeaPRISM because of the diverse viewing geometry generally relying on $\Delta\phi = 135^\circ$ instead of $\Delta\phi = 90^\circ$.

It is noted that the uncertainty for the sky glint correction is highly dependent on sea state and the relative percent value of this uncertainty is inversely proportional to $R_{rs}(\theta, \Delta\phi, \lambda)$ (see web appendix 2 of Ruddick et al., 2006). The values given here have, therefore, been calculated very specifically accounting for the sea state recorded during the ARC field activities and the observed water-leaving radiances (see Sect. 4). In fact measurements performed in different waters or sea state conditions may lead to different uncertainties.

TRIOS-E

The $L_T(\theta, \Delta\phi, \lambda)$, $L_i(\theta', \Delta\phi, \lambda)$ and $E_d(0^+, \lambda)$, measurements sequences are simultaneously recorded every 10 s for approximately 6 min, commonly using $\Delta\phi = 135^\circ$. The NIR-similarity correction is performed with $\lambda_1 = 720$ nm, $\lambda_2 = 780$ nm and $\alpha = 2.35$ (Ruddick et al., 2006). Rationale for choosing this wavelength pair, different from that applied for TRIOS-B, is the higher signal to noise ratio characterizing measurements at the shorter wavelengths.

Quality checks rely on the mode of $R_{rs}(555)$ for each measurement sequence. Data deviating by more than 10 % from the mode value are rejected; actually none of the clear sky data included in the ARC inter-comparison was discarded.

OSD
9, 787–833, 2012

Estimated uncertainties of $R_{rs}(\lambda)$ from TRIOS-E vary approximately within 4–6 % (see Table 7). The considered uncertainty sources are: (i) uncertainty of system calibration determined assuming the same irradiance standard is utilized for the absolute calibration of the E_d, L_T, and L_i sensors, and thus only accounting for effects of mechanical setup, inadequate baffling and reference plaque uncertainties (see Hooker et al., 2002b); (ii) uncertainty due to straylight effects quantified through the application of laboratory characterizations performed for RAMSES E_d, L_T and L_i sensors (Ansko, unpublished); (iii) polarization effects quantified as the maximum sensitivity to polarization determined through laboratory characterizations for RAMSES L_T and L_i sensors (Ruddick, unpublished); (iv) uncertainty in the turbid water NIR-similarity correction quantified accounting for 25 % of the applied corrections; (v) uncertainty in the correction for off-nadir viewing angle (also estimated as 25 % of the applied corrections); (vi) effects of non-cosine response of the E_d collector guessed from published data (Zibordi and Bulgarelli, 2007); (vii) environmental perturbations estimated from the variation coefficient of $R_{rs}(\lambda)$ from the same measurement sequence.

4 Data Analysis and results

The inter-comparison analysis has been performed using matchups (i.e., pair of data products from different systems) constructed by setting ±15 min maximum difference between measurements from the two systems/methods to be compared. Matchup analysis has been performed through the average of relative and of absolute values of relative percent differences. Specifically, the average of relative percent differences, RD, is computed as

$$\mathrm{RD} = 100\frac{1}{N}\sum_{n=1}^{N}\frac{\Re^{\mathrm{C}}(n)-\Re^{\mathrm{R}}(n)}{\Re^{\mathrm{R}}(n)}, \quad (16)$$

OSD
9, 787–833, 2012

while the average of absolute values of relative percent differences is given by

$$\mathrm{AD} = 100\frac{1}{N}\sum_{n=1}^{N}\frac{\left|\Re^{\mathrm{C}}(n)-\Re^{\mathrm{R}}(n)\right|}{\Re^{\mathrm{R}}(n)} \tag{17}$$

where N is the number of matchups, n is the matchup index, superscript C indicates the quantity to be compared and superscript R indicates the reference. While RD is applied as an index to measure biases, AD is applied to quantify scattering between compared values.

The root mean square of differences, RMS,

$$\mathrm{RMS} = \sqrt{\frac{1}{N}\sum_{n=1}^{N}\left(\Re^{\mathrm{C}}(n)-\Re^{\mathrm{R}}(n)\right)^2}\,. \tag{18}$$

is also included in the analysis as a statistical index to quantify absolute differences.

Data products from WiSPER are applied as the *reference*. This choice is only supported by the confidence acquired with the system and the related measurement method. WiSPER data for ARC inter-comparisons comprise measurements from 36 independent casts performed under clear sky conditions from 21–24 July 2010. Derived $L_{\mathrm{w}}(\lambda)$ spectra are given in Fig. 1. The shape of spectra suggests a water type characterized by moderate concentrations of phytoplankton and colored dissolved organic matter, as shown by the decrease of spectra from 555 nm toward 412 nm, and additionally moderate concentration of total suspended matter, as shown by non negligible values at 665 nm. An evaluation of the water type made in agreement with Loisel and Morel (1998), indicates the presence of Case 2 water during the whole field experiment. Values for relevant quantities describing measurement conditions are reported in Table 8. Specifically, measurements performed on water samples collected during ARC activities at the AAOT, indicate average Chl-*a* values of $0.9\pm0.3\,\mu\mathrm{g\,l^{-1}}$, concentrations of total suspended matter TSM of $1.8\pm0.4\,\mathrm{g\,l^{-1}}$ and absorption coefficient by colored dissolved organic matter a_y at 412 nm of $0.17\pm0.03\,\mathrm{m^{-1}}$. However, despite

OSD
9, 787–833, 2012

the relative constancy of near surface quantities, the analysis of $a(z,\lambda)$ and $c(z,\lambda)$ profile data collected simultaneously to WiSPER measurements with an AC-9 (WETLabs, Philomath), showed occasionally marked optical stratifications at depths comprised between 5 and 13 m. The exclusion from data processing of the measurements related to these depths enforced by quality tests applied to data from in-water systems/methods, has minimized possible inconsistencies in the inter-comparison of products potentially affected by the non-linear decay with depth of log-transformed $L_u(z,\lambda,t_0)$ and $E_d(z,\lambda,t_0)$ data.

By recalling that the objective of the inter-comparison is the evaluation of the overall performance of different systems/methods regularly applied for satellite ocean color validation activities, and not a detailed investigation of any individual method, a summary of inter-comparison results is presented through scatter plots in Figs. 2–4 for $L_w(\lambda)$, $E_d(0^+,\lambda)$ and $R_{rs}(\lambda)$, respectively. The different number of matchups included in the analysis for the various systems/methods, is explained by practical deployment issues for some systems on some days, the application of ±15 min threshold not always beeing reached because of inadequate synchronization of the start of measurement sequences or, like in the case of SeaPRISM data, justified by the automatic and fully asynchronous (when compared to ARC activities) execution of measurements. It is however reported that most of the TRIOS-B and TRIOS-E measurements used to construct matchups are within ±1 min from WiSPER measurements, while most of TACCS-S and TCCS-P measurements are within ±3 min.

Inter-comparisons of $L_w(\lambda)$ displayed in Fig. 2 exhibit root mean square of relative differences RMS in the range of 0.02–0.03 mW cm^{-2} µm^{-1} sr^{-1}, except TACCS-P reaching 0.04 mW cm^{-2} µm^{-1} sr^{-1}. Spectrally averaged values of RD and AD are generally within ±4 % and 5–7 %, respectively. Higher values (i.e., +9 and 10 %) are observed for TACCS-P. Determination coefficients, R^2, exhibit values higher than 0.98, except for the SeaPRISM data where $R^2 = 0.97$.

The inter-comparison results of $E_d(0^+,\lambda)$ shown in Fig. 3, also exhibit quite good results when considering the variety of instruments and also methods applied. In

OSD
9, 787–833, 2012

particular RMS are close to 5 mW cm^{-2} µm^{-1} for the above-water systems/methods and between 8 and 10 mW cm^{-2} µm^{-1} for TACCS-S and TACCS-P, respectively. The different performances of TRIOS and TACCS systems are explained by the diverse deployment methods: TRIOS $E_d(0^+,\lambda)$ measurements benefits from a fixed deployment platform while TACCS measurements are affected by the buoy motion adding geometric perturbations as a function of sea-state. The RMS value determined for SeaPRISM is comparable to those obtained for TRIOS. This result acquires particular relevance when considering that SeaPRISM $E_d(0^+,\lambda)$ data are determined theoretically from experimental values of $\tau_a(\lambda)$, a very different approach from actual measurements applied for all other systems/methods. Values of RD for $E_d(0^+,\lambda)$ are approximately within ±3 % while values of AD are close to 3 % for the above-water systems (e.g., SeaPRISM, TRIOS-B and TRIOS-E), but reach 5–7 % for the buoy-based systems/methods (i.e., TACCS-P and TACCS-S). Similarly, R^2 vary between 0.87 and 0.92 for the above-water systems, and exhibit much lower values for TACCS-P and TACCS-S (i.e., R^2 equal to 0.65 and 0.81, respectively).

The inter-comparison shown in Fig. 4 for $R_{rs}(\lambda)$ data exhibits results obviously depending on those obtained for $L_w(\lambda)$ and $E_d(0^+,\lambda)$ data. Specifically, lower RMS values (i.e., 0.0002 sr^{-1}) are shown for TRIOS-B and TRIOS-E, and the highest (i.e., 0.0004 sr^{-1}) for TACCS-P. RD values vary from −1 to +6 %, while AD values are approximately 6 % for the above-water systems and reach 9 % for the buoy-based systems. All R^2 vary between 0.95 and 0.99 with the lowest values again displayed by the TACCS-S and TACCS-P $R_{rs}(\lambda)$ as a result of the lower R^2 shown by $E_d(0^+,\lambda)$.

5 Discussion

Results for the ARC inter-comparison illustrate the best that can be achieved with the considered systems/methods under almost ideal measurement circumstances driven by favourable deployment capabilities as offered by the stability of the AAOT platform

OSD
9, 787–833, 2012

(i.e., making $E_d(0^+,\lambda)$ measurements unaffected by tilt, when performed from the main superstructure), almost ideal environmental conditions characterized by relatively low sun zenith angles, clear sky and moderately low sea state, and finally inter-calibration of measurement systems. By solely considering this latter element, it is recalled that the inter-calibration removes potential biases in derived radiometric products generated by out-of-date or inaccurate calibration factors. The comparison of absolute factors obtained at the JRC during the inter-calibration with those previously applied for the various systems included in ARC, has shown minimum differences of 1–2 % but also values exceeding 4 % for individual radiometers. These second relatively high differences, if not removed, would significantly degrade the inter-comparison for one of the considered system/method.

Processing of data from in-water systems/methods requires values of $a(\lambda)$ and $c(\lambda)$. Differently, processing of data from above-water systems/methods requires values W and Chl-*a*. The impact of uncertainties of these input quantities is accounted for in the $R_{rs}(\lambda)$ uncertainty budget for each system/method. It is however of interest to evaluate the impact of important quantities such as Chl-*a* utilized to correct for the off-nadir viewing geometry of $L_w(\lambda,\theta,\Delta\phi)$. In the present exercise Chl-*a* was determined for all systems using a regional algorithm (see Berthon and Zibordi, 2004) applied to $L_{wn}(\lambda)$ ratios. The average and the standard deviation of values computed for ARC measurements are $1.9 \pm 0.2\,\mu g\,l^{-1}$. The corresponding values for actual concentrations determined from water samples through High Pressure Liquid Chromatography (HPLC) are $0.9 \pm 0.3\,\mu g\,l^{-1}$. The analysis of TRIOS-B data indicates that the different Chl-*a* estimates give viewing angle corrections differing by less than 1 % for $\Delta\phi = 135^\circ$ and varying between 1 and 4 % for $\Delta\phi = 90^\circ$. However, the overall effect on $R_{rs}(\lambda)$ inter-comparisons is well within the assumed uncertainties. In fact, when using measured Chl-*a* instead of the computed values, TRIOS-E, TRIO-B and SeaPRISM results indicate an increase of 0.5 %, 0.9 % and 1.2 %, respectively, for the spectrally averaged RD and no significant change for the other statistical quantities. Differences among spectrally averaged RD for the various systems/methods are explained by the different

OSD
9, 787–833, 2012

measurement sequences included in the inter-comparison comprising diverse viewing geometries.

In order to evaluate the consistency of the overall inter-comparison results illustrated in Sect. 4, Table 9 displays spectral AD values determined for $R_{rs}(\lambda)$ at the 443, 555 and 665 nm center-wavelengths for the various systems/methods with respect to WiSPER, and the combined uncertainties (CU) determined from the statistical composition of uncertainties quantified for WiSPER $R_{rs}(\lambda)$ and for each other inter-compared system/method.

Recognizing that the computed CU values are overestimated by at least 1 % due to the inter-calibration of the various systems, the comparison is a way to evaluate the consistency of the uncertainty budgets quantified for each system/method. The agreement between AD and CU values adds confidence to the uncertainty values estimated for each system/method. The largest differences between AD and CU values are observed at 665 nm for a few systems/methods (see underlined values in Table 9). By pointing out that the low values of $R_{rs}(\lambda)$ at 665 nm (on the average 6 times lower than those observed at 555 nm) might easily lead to higher percent differences in the inter-comparison results with respect to shorter wavelengths, the largest AD (with respect CU values) are explained by biases affecting $L_w(665)$ with respect to WiSPER products (assumed as the true within the stated uncertainties). In fact an analysis of RD for $L_w(665)$ indicates a systematic underestimate of 20 % for TACCS-S and, a systematic overestimate of 21 % for TACCS-P and of 12 % for TRIOS-B. The reasons for these biases might be several. In the case of buoy-based systems it could be explained by the difficulty of accurately determining near surface $K_d(665)$, while in the case of TRIOS-B it could be explained by imperfect sky-glint removal. However, further investigations of these differences are beyond the scope of the work and likely out of the capabilities offered by the relatively small ARC data set tied to specific measurement conditions.

OSD
9, 787–833, 2012

6 Summary and conclusions

The agreement of spectral water-leaving radiance $L_w(\lambda)$, above-water downward irradiance $E_d(0^+,\lambda)$ and remote sensing reflectance $R_{rs}(\lambda)$ determined from various measurement systems and methods, has been investigated within the framework of a field inter-comparison called Assessment of In Situ Radiometric Capabilities for Coastal Water Remote Sensing Applications (ARC), carried out in the Northern Adriatic Sea. Taking advantage of the geometrically favourable deployment conditions offered by the Acqua Alta Oceanographic Tower, measurements were performed under almost ideal environmental conditions (i.e., clear sky, relatively low sun zeniths and moderately low sea state) with a variety of measurement systems embracing multispectral and hyperspectral optical sensors as well as in- and above-water methods. All optical sensors involved in the experiment, except one, were inter-calibrated through post-field absolute calibration with the same standards and methods. Data products from the various measurement systems/methods were directly compared to those from a single reference system/method. Overall inter-comparison results indicate an expected better performance for systems/methods relying on stable deployment platforms and thus exhibiting lower uncertainties in $E_d(0^+,\lambda)$. Results for $R_{rs}(\lambda)$ indicate spectrally averaged relative differences generally within −1 and +6 %. Spectrally averaged values of the absolute of relative differences are approximately 6 % for the above-water systems/methods, and increase to 9 % for the buoy-based systems/methods. The general agreement of this latter spectral $R_{rs}(\lambda)$ uncertainty index with the combined uncertainties of inter-compared systems/methods is notable. This result undoubtedly confirms the consistency of the evaluated data products and provides confidence in the capability of the considered systems/methods to generate radiometric products within the declared range of uncertainties. However, it must be recalled that all measurements were performed under almost ideal conditions and for a limited range of environmental situations. Additionally, all the optical sensors benefitted from a common laboratory radiometric inter-calibration. These elements are specific to the ARC activity and

OSD
9, 787–833, 2012

there is no assurance of achieving equivalent results with the considered systems and methods when using fully independent absolute radiometric calibrations, performing deployments from ships rather than grounded platforms (where applicable) or carrying out measurements during more extreme environmental conditions (e.g., elevated sun zenith angles, high sea state, water column characterized by near-surface gradient of optical properties, partially cloudy sky). This final consideration further supports the relevance and need for regular inter-comparison activities as best practice to comprehensively investigate uncertainties of measurements devoted to the validation of primary satellite ocean color products and mainly those going to be included in common repositories (e.g., Meris Matchup In situ Database (MERMAID) and SeaWiFS Bio-optical Archive and Storage System (SeaBASS)).

Acknowledgements. Jean-Paul Huot and Philippe Goryl from ESA are duly acknowledged for the support provided to the ARC activity within the framework of the MERIS Validation Team activities. The authors are equally grateful to Nigel Fox, chair of the IVOS subgroup of CEOS-WGCV, for stimulating the activity and managing any related administrative issue. The authors also wish to thank the NASA AERONET team led by Brent Holben for the continuous effort in supporting AERONET-OC. Acknowledgments are finally due to Jean-François Berthon, Elisabetta Canuti, Lukasz Jankowski, José Beltrán and Agnieszka Bialek for the support provided during various phases of the inter-comparison. Kevin Ruddick's participation was partially funded by the Belgian Science Policy Office STEREO Programme under the BELCOLOUR-2 (SR/00/104) contract.

References

Achard F., Eva, H. D., Stibig, H. J., Mayaux, P., Gallego, J., Richards., T., and Malingreau. J. P.: Determination of deforestation rates of the world's humid tropical forests Science, 297, 999, 2002.

Austin, R. W.: The remote sensing of spectral radiance from below the ocean surface, in: Optical Aspects of Oceanography, Academic Press, London and New York, 1974.

Barton, I. J., Minnet, P. J., Maillet, K. A., Donlon, C. J., Hook, S. J., Jessup, A. T., and Nightin-

OSD

9, 787–833, 2012

gale, T. J.: The Miami2001 infrared radiometer calibration and intercomparison. Part II: Shipboard results, J. Atmos. Ocean. Tech., 21, 268–283, 2004.
Behrenfeld, M. J., O'Malley, R. T., Siegel, D. A., McClain, C. R., Sarmiento, J. L., Feldman, G. C., Milligan A. J., Falkowski, P. G., Letelier, R. M., and Boss, E. S.: Climate-driven trends in contemporary ocean productivity, Nature, 444, 752–755, 2006.
Berthon, J.-F. and Zibordi, G.: Bio-optical relationships for the Northern Adriatic Sea Int. J. Remote Sens., 25, 1527–1532, 2004.
Bird, R. E. and Riordan, C. J.: Simple solar spectral model for direct and diffuse irradiance on horizontal and tilted planes at the Earth's surface for cloudless atmospheres J. Clim. Appl. Meteorol., 25, 87–97, 1986.
Brando, V. E. and Dekker, A. G.: Satellite hyperspectral remote sensing for estimating estuarine and coastal water quality, IEEE T. Geosci. Remote, 41, 1378–1387, 2003.
Deschamps, P.-Y., Fougnie, B., Frouin, R., Lecomte, P., and Verwaerde, C.: SIMBAD: a field radiometer for satellite ocean-color validation, Appl. Optics, 43, 4055–4069, 2004.
Doyle, J. P. and Zibordi, G.: Optical propagation within a 3-dimensional shadowed atmosphere-ocean field: application to large deployment structures, Appl. Optics, 41, 4283–4306.
D'Alimonte, D., Zibordi, G., Kajiyama, T., and Cunha, J. C.: A Monte Carlo code for high spatial resolution ocean color simulations, Appl. Optics, 49, 4936–4950, 2002.
Fougnie. B., Frouin, R., Lecomte, P., and Deschamps, P. Y.: Reduction of skylight reflection effects in the above-water measurement of diffuse marine reflectance, Appl. Optics, 38, 3844–3856, 1999.
Gordon, H. and Clark, D. K.: Clear water radiances for atmospheric correction of Coastal Zone Color Scanner imagery, Appl. Optics, 20, 4175–4180, 1981.
Gordon, H. and Ding, K.: Self-shading of in-water optical measurements Limnol. Oceanogr., 37, 491–500, 1992.
Hooker, S. B., Lazin, G., Zibordi, G., and McClean, S.: An evaluation of above- and in-water methods for determining water leaving radiances J. Atmos. Ocean. Tech., 19, 486–515, 2002a.
Hooker, S. B., McLean, S., Small, M., Lazin, G., Zibord, I. G., and Brown, J.: The Seventh SeaWiFS Intercalibration Round-Robin Experiment (SIRREX-7), March 1999. SeaWiFS Report NASA/TM-2001–206892, vol. 17, edited by: Hooker, S. B. and Firestone, E. R., NASA Goddard Space Flight Center, Greenbelt, Maryland, 2002b.
Hooker, S. B., Zibordi, G., Berthon, J.-F., and Brown, J. W.: Above-water radiometry in shallow

OSD
9, 787–833, 2012

coastal waters, Appl. Optics, 43, 4254–4268, 2004.
Hooker, S. B. and Zibordi, G.: Platform perturbation in above-water radiometry, Appl. Optics, 44, 553–567, 2005.
Kaufman, Y. J., Tanré, D., and Boucher, O.: A satellite view of aerosols in the climate system, Nature, 419, 215–223, 2002.
Kirk, J. T. O.: Light and Photosynthesis in Aquatic Ecosystems, 2nd edn., Cambridge University Press, Cambridge, 1994.
Loisel, H. and Morel, A.: Light scattering and chlorophyll concentration in Case 1 waters: a re-examination, Limnol. Oceanogr., 43, 847–858, 1998.
Mobley, C. D.: Hydrolight 4.0 Users Guide DTIC Document, Sequoia Scientific, Inc., Bellevue, WA., 1998.
Mobley, C. D.: Estimation of the remote sensing reflectance from above-water methods, Appl. Optics, 38, 7442–7455, 1999.
Moore, G. F., Icely, J. D., and Kratzer, S.: Field inter-comparison and validation of in-water radiometer and sun photometers for MERIS validation, Proc. ESA Living Planet Symposium, Special Publication SP-686, European Space Agency, Noordwijk, 2011.
Morel, A. and Antoine, D.: Heating rate within the upper ocean in relation to its bio-optical state, J. Phys. Oceanogr., 24, 1652–1665, 1994.
Morel, A., Antoine, D., and Gentili, B.: Bidirectional reflectance of oceanic waters: accounting for Raman emission and varying particle scattering phase function, Appl. Optics, 41, 6289–6306, 2002.
Mueller. J. L. and Fargion, G.: Ocean Optics Protocols for Satellite Ocean Color Sensor Validation, Revision 3. NASA/TM-2002–210004/Rev3, Greenbelt, NASA Goddard Space Flight Center, 2002.
Petzold, T. J.: Volume scattering functions for selected ocean waters, Scripps Institution of Oceanography, La Jolla, San Diego, SIO Ref. 72–78, 1972.
Ruddick, K., De Cauwer, V., and Van Mol, B.: Use of the near infrared similarity spectrum for the quality control of remote sensing data. SPIE International Conference 5885 on Remote Sensing of the Coastal Oceanic Environment, San Diego, 31 July–01 August, 2005.
Ruddick, K., De Cauwer, V., Park, Y., and Moore, G.: Seaborne measurements of near infrared water-leaving reflectance – the similarity spectrum for turbid waters, Limnol. Oceanogr., 51, 1167–1179, 2006.
Ruddick, K., Lacroix, G., Lancelot, C., Nechad, B., Park, Y., Peters, S., and Van Mol, B.: Optical

OSD
9, 787–833, 2012

remote sensing of the North Sea, in: Remote Sensing of the European Seas, edited by: Barale, V. and Gade, M., Springer Science + Business Media B.V., 79–90, 2008.
Stroeve, J., Holland, M. M., Meier, W., Scambos, T., and Serreze, M.: Arctic sea ice decline: Faster than forecast, Geophys. Res. Lett., 34, L09501, doi:10.1029/2007GL029703, 2007.
Stumpf, R. P. and Tomlinson, M. C.: Remote sensing of harmful algae blooms, in: Remote Sensing of Coastal Aquatic Environments: Technologies, Techniques and Applications, edited by: Miller, R., Castillo, C. D., and McKee, B., Springer, Dordrecht, 2005.
Thome, K., Schiller, S., Conel, J., Arai, K., and Tsuchida, S.: Results of the 1996 Earth observing system vicarious calibration joint campaign to Lunar Lake Playa, Nevada (USA), Metrologia, 35, 631–638, 1998.
Thuillier, G., Hersé, M., Labs, D., Foujols, T., Peetermans, W., Gillotay, D., Simon, P. C., and Mandel, H.: The solar spectral irradiance from 200 to 2400 nm as measured by the SOLSPEC spectrometer from the Atlas and Eureca missions, Sol. Phys., 214, 1–22, 2003.
Zaneveld, J. R., Boss, V. E., and Barnard, A.: Influence of surface waves on measured and modeled irradiance profiles, Appl. Optics, 40, 1442–1449, 2001.
Zibordi, G.: Immersion factor of in-water radiance sensors: assessment for a class of radiometers, J. Atmos. Ocean. Tech., 23, 302–313, 2006.
Zibordi, G. and Ferrari, G. M.: Instrument self shading in underwater optical measurements: experimental data, Appl. Optics, 34, 2750–2754, 1995.
Zibordi, G. and Bulgarelli, B.: Effects of cosine error in irradiance measurements from field ocean color radiometers, Appl. Optics, 46, 5529–5538, 2007.
Zibordi, G., Doyle, G. P., and Hooker, S. B.: Offshore tower shading effects on in-water optical measurements, J. Atmos. Ocean. Tech., 16, 1767–1779, 1999.
Zibordi, G., Hooker, S. B., Berthon, J.-F., and D'Alimonte, D.: Autonomous above-water radiance measurement from an offshore platform: a field assessment, J. Atmos. Ocean. Tech., 19, 808–819, 2002.
Zibordi, G., D'Alimonte, D., and Berthon, J.-F.: An evaluation of depth resolution requirements for optical profiling in coastal waters, J. Atmos. Ocean. Tech., 21, 1059–1073, 2004a.
Zibordi, G., Mélin, F., Hooker, S. B., D'Alimonte, D., and Holben, B.: An autonomous above-water system for the validation of ocean color radiance data, IEEE T. Geosci. Remote, 42, 401–415, 2004b.
Zibordi, G., Mélin, F., and Berthon, J.-F.: Comparison of SeaWiFS, MODIS and MERIS radiometric products at a coastal site, Geophys Res. Lett., 33, L06617,

OSD
9, 787–833, 2012

doi:10.1029/2006GL25778, 2006.
Zibordi, G., Berthon, J.-F., and D'Alimonte, D.: An evaluation of radiometric products fixed-depth and continuous in-water profile data from a coastal site, J. Atmos. Ocean. Tech., 26, 91–186, 2009a.
Zibordi, G., Berthon, J.-F., Mélin, F., D'Alimonte, D., and Kaitala, S.: Validation of satellite ocean color primary products at optically complex coastal sites: Northern Adriatic Sea, Northern Baltic Proper and Gulf of Finland, Remote Sens. Environ., 113, 2574–2591, 2009b.
Zibordi, G., Holben, B., Slutsker, I., Giles, D., D'Alimonte, D., Mélin, F., Berthon, J.-F., Vandemark, D., Feng, H., Schuster, G., Fabbri, B. E., Kaitala, S., and Seppälä, J.: AERONET-OC: a network for the validation of Ocean Color primary radiometric products, J. Atmos. Ocean. Tech., 26, 1634–1651, 2009c.

OSD
9, 787–833, 2012

Table 1. Summary of codes assigned to measurement systems/methods together with relevant references, main input quantities required for data processing, and responsible institutes (symbols r, a and c indicate the above-water diffuse to direct irradiance ratio, the seawater absorption and beam attenuation coefficients, respectively).

System/method code (type)	Measurement system	References for system/method	Main input quantities	Responsible institutes(s)
WiSPER (in-water)	Wire-Stabilized Profiling Environmental Radiometer (WiSPER)	Zibordi et al. (2004c), Zibordi et al. (2009a)	$L_u(z,\lambda,t)$, $E_d(0^+,\lambda,t)$, $a(0^-,\lambda)$, $c(0^-,\lambda)$, $r(0^+,\lambda)$	Joint Research Centre
TACCS-S (in-water)	Tethered Attenuation Coefficient Chain Sensor (TACCS)	Moore et al. (2011)	$L_u(z_i,\lambda,t)$, $E_d(z_i,\lambda,t)$, $E_d(0^+,\lambda,t)$, $a(z,\lambda)$, $c(z,\lambda)$	Stockholm University and Bio-Optika
TACCS-P (in-water)	Tethered Attenuation Coefficient Chain Sensor (TACCS)	Moore et al. (2011)	$L_u(z_i,\lambda,t)$, $E_d(z_i,\lambda,t)$, $E_d(0^+,\lambda,t)$, $a(0^-,\lambda)$, $c(0^-,\lambda)$, $r(0^+,\lambda)$	Sagremarisco Lda and Bio-Optika
SeaPRISM (above-water)	SeaWiFS Photometer Revision for Incident Surface Measurements (SeaPRISM)	Zibordi et al. (2004b), Zibordi et al. (2009c)	$L_T(\theta,\Delta\phi,\lambda)$, $L_i(\theta',\Delta\phi,\lambda)$, $E(\theta_0,\phi_0,\lambda)$, W, Chl-a, $\tau_a(\lambda)$	Joint Research Centre
TRIOS-B (above-water)	RAMSES Hyperspectral Radiometers (TRIOS)	Ruddick et al. (2005), Ruddick et al. (2006)	$L_T(\theta,\Delta\phi,\lambda)$, $L_i(\theta',\Delta\phi,\lambda)$, $E_d(0^+,\lambda,t)$, W, Chl-a	Management Unit of the North Sea Mathematical Models
TRIOS-E (above-water)	RAMSES Hyperspectral Radiometers (TRIOS)	Ruddick et al. (2005), Ruddick et al. (2006)	$L_T(\theta,\Delta\phi,\lambda)$, $L_i(\theta',\Delta\phi,\lambda)$, $E_d(0^+,\lambda,t)$, W, Chl-a	Tartu Observatory

OSD
9, 787–833, 2012

Table 2. Uncertainty budget (in percent) for R_{rs} determined from WiSPER data at selected center-wavelengths.

Uncertainty source	443	555	665
Absolute calibration of $L_u(z,\lambda,t)$	2.8	2.8	2.8
Self- and tower-shading corrections	3.0	1.8	3.2
Absolute calibration of $E_d(0^+,\lambda)$	2.5	2.5	2.5
Environmental perturbations	0.7	0.7	0.8
Quadrature sum	4.9	4.2	5.0

OSD
9, 787–833, 2012

Table 3. Uncertainty budget (in percent) for R_{rs} determined from TACCS-S data at selected center-wavelengths.

Uncertainty source	443	560	670
Absolute calibration of $L_u(z_0,\lambda,t)$	2.8	2.8	2.8
Self-shading correction	1.2	1.5	4.3
Absolute calibration of $E_d(0^+,\lambda)$	3.1	3.1	3.1
Interpolation of missing $E_d(0^+,\lambda)$	0.0	2.0	0.0
Bio-optical assumptions	2.2	2.3	3.7
Geometrical effects	4.5	4.0	3.0
Environmental perturbations	1.1	1.1	1.9
Quadrature sum	6.7	6.8	7.9

OSD
9, 787–833, 2012

Table 4. Uncertainty budget (in percent) for R_{rs} determined from TACCS-P data at selected center-wavelengths.

Uncertainty source	443	555	665
Absolute calibration of $L_u(z_0,\lambda,t)$	2.8	2.8	2.8
Self-shading correction	0.7	0.7	2.8
Absolute calibration of $E_d(0^+,\lambda)$	3.1	3.1	3.1
Bio-optical assumptions	2.2	2.0	2.0
Geometrical effects	4.5	4.0	3.0
Environmental perturbations	1.8	1.9	3.9
Quadrature sum	6.8	6.4	7.3

OSD
9, 787–833, 2012

Table 5. Uncertainty budget (in percent) for R_{rs} determined from SeaPRISM data at selected center-wavelengths.

Uncertainty source	443	555	665
Absolute calibration	2.7	2.7	2.7
Viewing-angle correction	2.2	2.0	2.2
Uncertainties in $t_d(\lambda)$, $\rho(\theta)$, W	2.1	1.7	2.9
Uncertainties in $E_0(\lambda)$	1.6	0.7	0.1
Environmental perturbations	2.0	1.9	8.7
Quadrature sum	4.5	4.2	9.8

OSD
9, 787–833, 2012

Table 6. Uncertainty budget (in percent) for R_{rs} determined from TRIOS-B data at selected center-wavelengths.

Uncertainty source	443	555	665
System calibration	2.0	2.0	2.0
Straylight effects	5.0	0.5	1.0
Polarization effects	1.0	1.0	1.0
Non-cosine response of E_d	2.0	2.0	2.0
Sky-light correction	2.0	1.0	2.9
Viewing angle correction	1.5	1.5	1.5
Quadrature sum	6.3	3.5	4.5

OSD
9, 787–833, 2012

Table 7. Uncertainty budget (in percent) for R_{rs} determined from TRIOS-E data at selected center-wavelengths.

Uncertainty source	443	555	665
System calibration	2.0	2.0	2.0
Straylight effects	5.0	0.5	1.0
Polarization effects	1.0	1.0	1.0
NIR-similarity correction	0.5	0.4	2.2
Viewing angle correction	1.5	1.7	1.3
Non-cosine response of E_d	2.0	2.0	2.0
Environmental perturbations	1.8	1.0	2.0
Quadrature sum	6.3	3.6	4.5

OSD
9, 787–833, 2012

Table 8. Value of major quantities characterizing the measurement conditions during ARC activities at the AAOT.

Quantity	Mean ± Std	Range (min-max)
$L_w(490)$ (mW cm^{-2} µm^{-1} sr^{-1})	0.64 ± 0.09	0.51–0.81
$K_d(490)$ (m^{-1})	0.19 ± 0.02	0.16–0.22
$a_y(412)$ (m^{-1})	0.17 ± 0.03	0.13–0.20
Chl-*a* (µg $^{-1}$)	0.9 ± 0.3	0.6–1.5
TSM (mg l^{-1})	1.8 ± 0.4	1.3–2.4
Wind speed (m s^{-1})	2.9 ± 1.1	0.9–4.5
Sun zenith (degrees)	30.3 ± 5.2	24.6–43.1
Cloud cover (octs)	0 ± 0	0–0

OSD
9, 787–833, 2012

Table 9. Average values of the absolute of relative percent differences (AD) determined for $R_{rs}(\lambda)$ at the 443, 555 and 665 nm center-wavelengths for the various systems/methods with respect to WiSPER, and combined uncertainties (CU) determined from the statistical composition of uncertainties quantifies for $R_{rs}(\lambda)$ derived from WiSPER and from each other inter-compared system/method. Underlined values indicate AD significantly greater than the computed CU values.

	AD (%)			CU (%)		
λ	443	555	665	443	555	665
TACCS-S	4.5	6.1	<u>21.2</u>	8.3	8.0	9.3
TACCS-P	8.7	7.8	<u>16.1</u>	8.4	7.7	8.8
SeaPRISM	5.7	6.0	7.6	6.9	6.0	11.0
TRIOS-B	7.7	2.7	<u>11.0</u>	8.0	5.5	6.7
TRIOS-E	5.9	3.9	7.2	8.0	5.5	6.7

OSD
9, 787–833, 2012

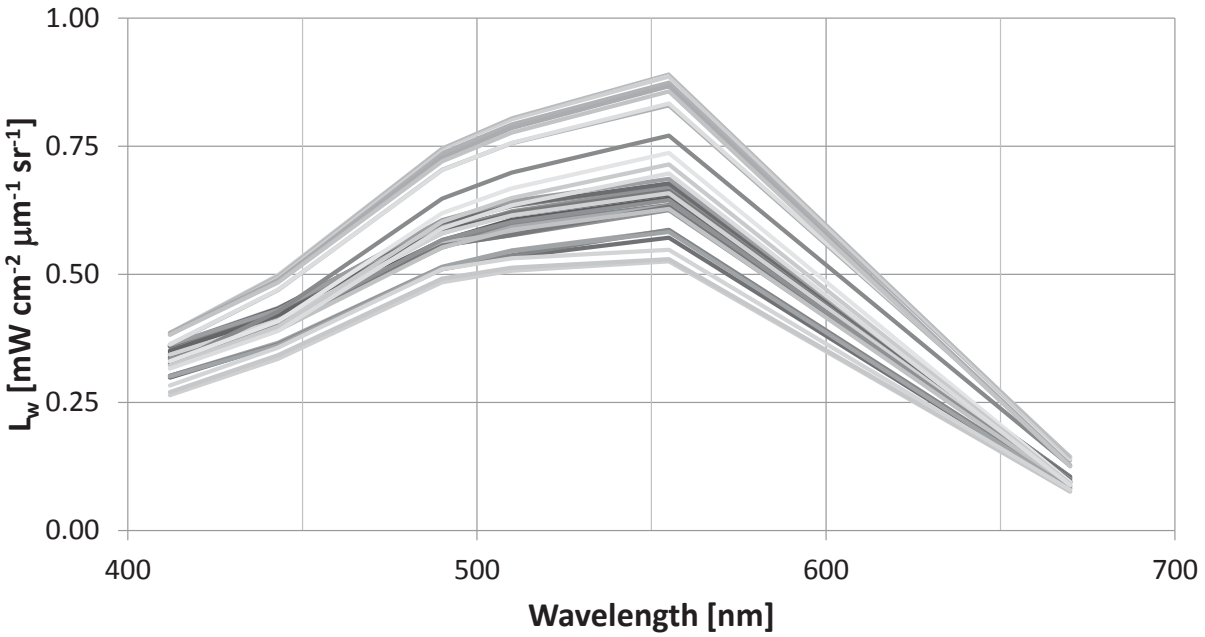

Fig. 1. $L_w(\lambda)$ spectra produced during the ARC experiment at the AAOT from WiSPER profile data.

OSD
9, 787–833, 2012

In situ determination of the remote sensing reflectance: an inter-comparison

G. Zibordi et al.

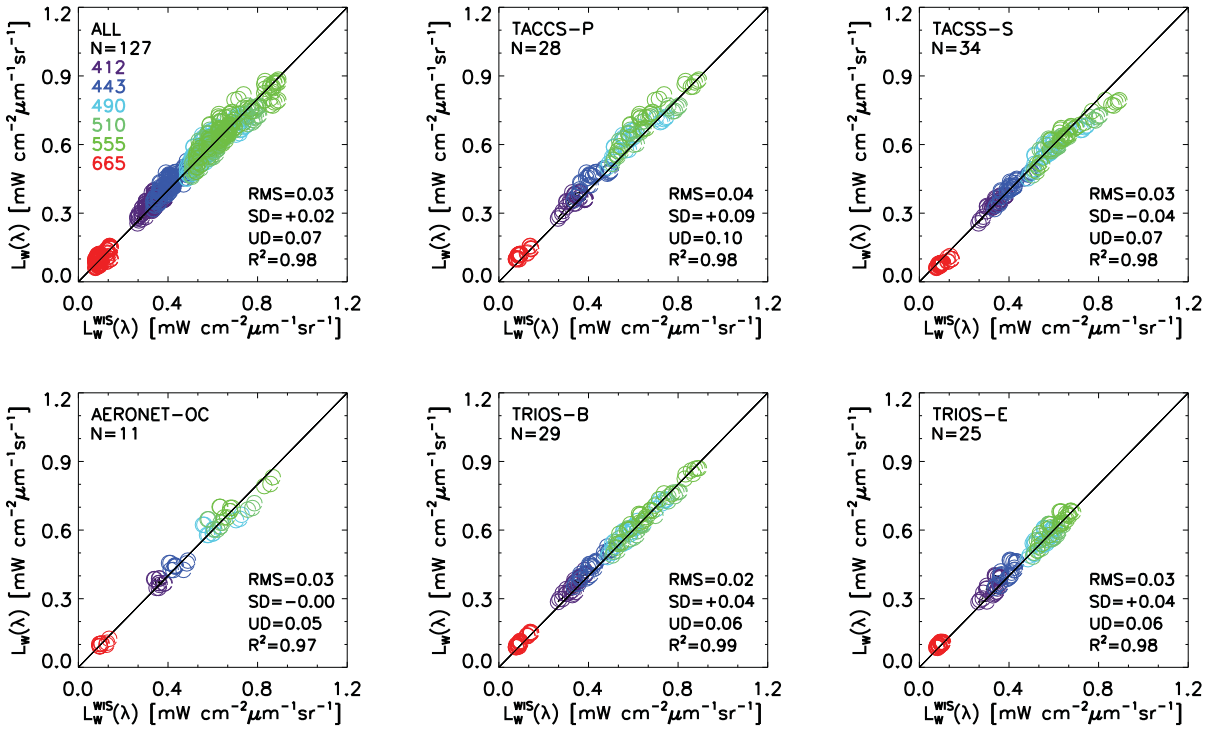

Fig. 2. Scatter plots of $L_w(\lambda)$ from the various systems-methods versus $L_w(\lambda)$ from WiSPER (ALL indicates merged data from all individual inter-comparisons). RMS indicates the spectrally averaged root mean square of differences, while RD and AD in % indicate spectrally averaged values of relative differences and of absolute values of relative differences, respectively. *N* is the number of matchups obtained assuming a ±15 min maximum difference between measurements. Diverse colors indicate data at different center-wavelengths.

OSD
9, 787–833, 2012

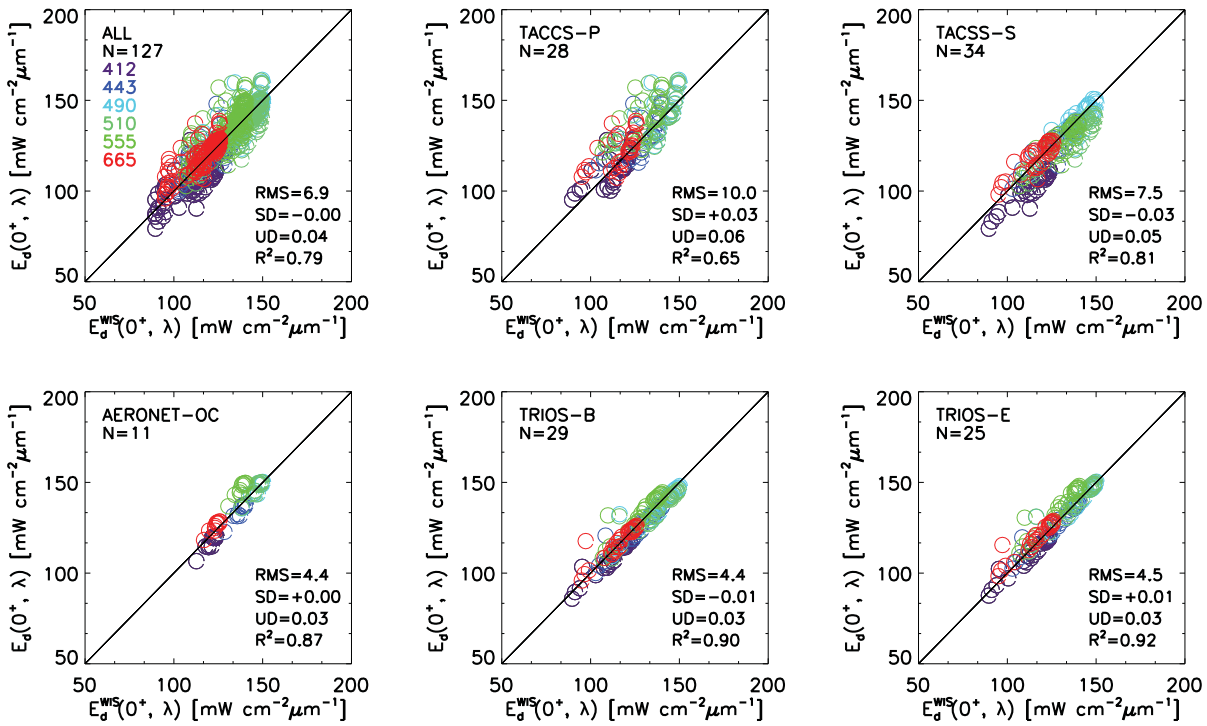

Fig. 3. As in Fig. 2 but for $E_d(0^+,\lambda)$.

OSD
9, 787–833, 2012

In situ determination of the remote sensing reflectance: an inter-comparison

G. Zibordi et al.

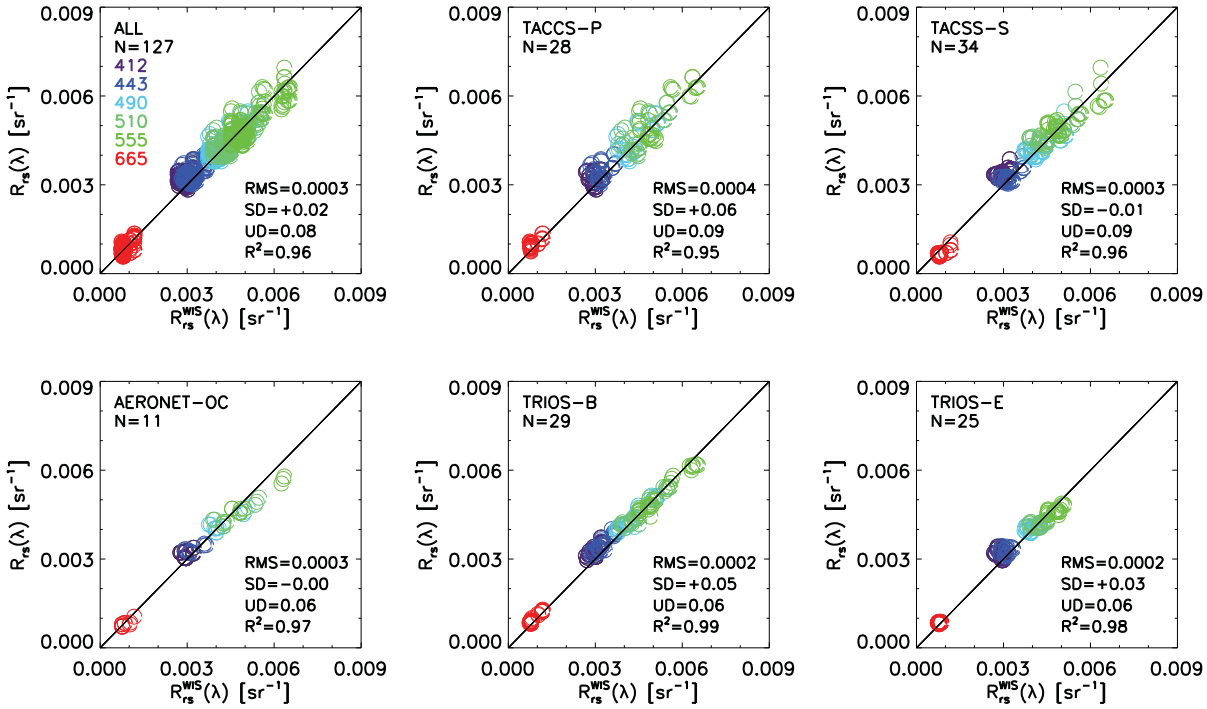

Fig. 4. As in Fig. 2 but for $R_{rs}(\lambda)$.

OSD
9, 787–833, 2012

In situ determination of the remote sensing reflectance: an inter-comparison

G. Zibordi et al.